ISSN 1560-0904, Polymer Science, Series B, 2019, Vol. 61, No. 3, pp. 376–386. © Pleiades Publishing, Ltd., 2019.

COMPOSITES

A Novel pH, Thermo, and Magnetic Responsive Hydrogel Nanocomposite Containing Nanogel for Anticancer Drug Delivery[1]

Somayeh Ghavami[a], Ghasem Rezanejade Bardajee[a,*], Ahmad Mirshokraie[a], and Khadijeh Didehban[a]

[a] *Department of Chemistry, Payame Noor University, Tehran, 19395-3697 Iran*

**e-mail: rezanejad@pnu.ac.ir*

Received June 14, 2018; revised September 28, 2018; accepted December 19, 2018

Abstract—Hydrogels, nanogels, and nanocomposites have attracted much attention as drug delivery systems during the past decades. In this work, a novel drug delivery system was synthesized by incorporation of nanogel into multi responsive hydrogel nanocomposite. At first, nanogel was prepared by copolymerization of *N*-isopropylacrylamide (NIPAM) and (2-dimethylamino)ethyl methacrylate (DMA). Then it was embedded it into pH, thermo, and magnetic responsive hydrogel nanocomposite including graft copolymerization of poly(2-dimethylamino)ethyl methacrylate (PDMA) onto salep (PDMA-*g*-salep) and Fe_3O_4 nanoparticles (NPs). The synthesized samples were characterized by Fourier transform infrared spectroscopy (FTIR), thermo gravimetric analysis (TGA), X-ray diffraction (XRD), scanning electron microscopy (SEM), vibrating sample magnetometer (VSM), and atomic force micrographs (AFM). The sensitivity of the synthesized sample to temperature, pH, and magnetic field was studied using the swelling experiments. The drug release ability of the sample was also investigated at different pH, temperatures, and magnetic field. Finally, different kinetic models were used to discuss about the mechanism of drug release from the prepared sample. Our results represented the high efficiency of this kind of hydrogel nanocomposite for applications in cancer therapy.

DOI: 10.1134/S1560090419030047

INTRODUCTION

Anticancer drugs play important roles in cancer treatment [1]. However, these drugs have many disadvantages such as poor solubility, high toxicity, and serious side effects like hair loss, nausea, and vomiting [2–5]. To overcome these drawbacks, many attempts have been made to develop novel controlled drug delivery systems [4, 5]. They can encapsulate of the drug and release it to the cancer site without leaking into other sites [6–8]. The employment of multi-responsive hydrogels as an drug delivery system have advantages over other drug delivery systems because of their ease of preparation, high efficiency, high-water content, tunable physical, and biological properties [9, 10]. The most advantage of these hydrogels is a volume phase transitions in their cross-linked three-dimensional networks as exposure to external stimuli such as temperature, pH, pressure, electric field, magnetic field, and light [11]. In particular, polysaccharides like starch, salep, alginate, carrageenan, dextran, heparin, gum Arabic, and agarose have a great potential for the development of multi-responsive hydrogel owing to their low toxicity, good biocompatibility, excellent biodegradability, clinical tolerability, and efficient absorption [12–15].

Besides, all these advantages, multi-responsive hydrogels based on polysaccharides suffer from some serious limitations like relatively rapid release of drugs from hydrogel, low stability, and low mechanical property for their further application in biomedical field [16–18]. The relatively rapid release of drug from hydrogel is due to their high water content and large pore sizes [19]. Some researchers reported that the incorporation of microgel or nanogel into the hydrogel eliminated the initial burst release of hydrogel and improved the kinetic drug release profile [20–22]. Gil et al. synthesized cisplatin-bearing chondroitin sulfate nanogels (CS-nanogels), and incorporated them into pH- and temperature-responsive bioresorbable poly(ethylene glycol-poly(*b*-aminoester urethane) hydrogels for cancer cell-specific delivery of cisplatin (CDDP) [20]. Their results showed that the CDDP released slowly from the hydrogels at pH 7.4, whereas the CDDP release was triggered at pH 5.0. Our results showed that the formation of Fe_3O_4 NPs into hydrogel networks leads to innovative materials with exceptional characteristics not present in either component [21]. They found that the obtained hybrid hydrogel enables the release of the dextrin nanogel over an

[1] The article is published in the original.

extended period, paralleling the mass loss curve due to the degradation of the material. Lehmann et al. prepared thermosensitive composite hydrogels that consist of a poly(acrylamide) hydrogel matrix with embedded micrometer-sized poly(*N*-isopropylacrylamide) microgel as promising models for complex, heterogeneous gels [22]. They investigated mobility of nanoscopic dextran tracers within the gels and showed the mobility of dextran tracers inside the embedded microgel beads is hindered compared to those in free beads and in the surrounding gel matrix.

The low stability and low mechanical property of hydrogel is attributed to preparing hydrogel with chemical crosslinking agent like *N*,*N*-methylene-*bis*-acrylamide (MBA) [23, 24]. To resolve this problem, Fe_3O_4 nanoparticles (NPs) are mixed with the polymeric network to form physical crosslinking with polymer chains through hydrogen bond, ionic bond or coordination bond [25, 26]. Fe_3O_4NPs are one of the most common iron oxide materials that reveal wonderful physico-chemical properties owing to the presence of both Fe(II) and Fe(III) in its structure [27]. In addition, they are non-toxic materials, bio-compatible, and biological degradable for use in biomedical applications such as MRI contrast enhancement agents, hyperthermia treatment, and drug delivery system [25–27]. For example, Zhou et al. explored the use of Fe_3O_4 NPs as a crosslinking agent to form poly(vinyl alcohol) (PVA) gel and used the prepared gel for drug delivery application [28]. In this processes the mixed aqueous solution of iron salts and PVA solution were added dropwise into alkaline solution to simultaneously formation of Fe_3O_4 NPs and crosslink of PVA chains. In our previous works, we synthesized various biocompatible hydrogel nanocomposites based on salep, kappa carrageenan, and starch using Zhou et al. method for targeted drug release [29–31]. Our results showed that the formation of Fe_3O_4 NPs into hydrogel networks leads to innovative materials with exceptional characteristics not present in either component. However, their drug release behavior was required to enhance in order to extend its applications in biomedical areas.

Therefore, we encouraged to design and to synthesize a novel drug delivery system by incorporation of nanogel into multi responsive hydrogel nanocomposite. In this work, at first, we prepared nanogels by copolymerization of *N*-isopropylacrylamide (NIPAM) and (2-dimethylamino) ethyl methacrylate) (DMA) and then incorporated them into pH, thermo, and magnetic responsive hydrogel nanocomposite including graft copolymerization of PDMA onto salep (PDMA-*g*-salep) and Fe_3O_4 NPs. The structures and various properties of the prepared samples were systematically characterized by Fourier transform infrared spectroscopy (FTIR), thermogravimetric analysis (TGA), X-ray diffraction (XRD), scanning electron microscopy (SEM), vibrating sample magnetometer (VSM), and atomic force micrographs (AFM). The swelling behavior of the obtained hydrogel nanocomposite was investigated at different times, temperatures, and pH. In addition, their application for controlled release of doxorubicin hydrochloride (DOX) drug was investigated. This study will be useful for further research and practical applications of the hydrogel nanocomposite in drug delivery systems.

EXPERIMENTAL

Materials

Salep was purchased from a supplier in Kordestan, Iran ($M_n = 1.17 \times 10^6$, $M_w = 1.64 \times 10^6$ (high M_w), PDI = 1.39, eluent = water, flow rate = 1 mL/min, acquisition interval = 0.43 s from GPC results). Reagents including sodium dodecylsulfate (SDS), MBA, NIPAM, DMA, ferric chloride hexahydrate ($FeCl_3 \cdot 6H_2O$), ferrous chloride tetrahydrate ($FeCl_2 \cdot 4H_2O$), and DOX were purchased from Sigma-Aldrich, Germany. Ammonium persulfate (APS) was obtained from Fluka, USA. All chemicals were at least of analytical reagent grade and used as received. Double distilled water was used in all the processes of aqueous solution preparations and washings.

Characterization

Fourier transform infrared (FTIR) spectra were collected in the wave number ranging from 400–4000 cm^{-1} using a Jasco 4200 FTIR spectrophotometer. X-ray diffraction (XRD) was performed using a D/Max-IIIA XRD analyzer equipped with a CuK_α monochromatic radiation source. Thermo gravimetric analysis (TGA) was measured for powder samples (about 10 mg) using a TA instrument 2050 thermo-gravimetric (TG) analyzer at a heating rate 20 grad/min, nitrogen flux. The UV–Vis absorption spectra of the samples were recorded on a Shimadzu UV–Vis 1650 PC spectrophotometer. Scanning electron microscopy (SEM) examination was achieved on a Hitachi S-5200 SEM at an acceleration voltage of 10 kV. Vibrating sample magnetometer (VSM) was performed using the Model 880 from ADE technologies, USA. Atomic force micrographs (AFM) were obtained using an AFM; SPI3800, Seiko Instruments, Japan.

Synthesis of PDN-Nanogel and DOX/PDN-Nanogel

PDN-nanogel was synthesized by a facile method as follows. First MBA (0.1 g), SDS (0.05 g), DMA (4 mL), and NIPAM (0.5 g) was quickly mixed in 45 mL double distilled water under strong stirring and Ar purge at to 80°C. After 30 min, APS (0.03 g in 2 mL water) was added to the mixture and the reaction was allowed to proceed for 4 h. Then, the product was centrifuged and washed with water. The water was used as solvent and for washing the product as well. Finally,

the obtained nanogel was dried in a vacuum at 40°C. Just vacuum was used to dry the final product.

Referring to the preparation procedure of PDN-nanogel, the mixture of MBA (0.1 g), SDS (0.05 g), DMA (4 mL), and NIPAM (0.5 g) in 45 mL double distilled water under strong stirring and Ar purge at to 80°C was synthesized. It was note that the PDN-nanogel did not dissolve in water. Then, 1 mL DOX solution (2 mg/mL) was added. The mixture was stirred for 30 min and then APS (0.03 g in 2 mL water) was added to the mixture and the reaction was allowed to proceed for 4 h. Then, the product was centrifuged to remove unloaded drug. An UV–Vis spectrometer was used to detect the absorption of the media for indirect determination of the DOX encapsulation efficiency. After being washed with double distilled water, the sample was dried in a vacuum at 40°C.

Synthesis of PDN-Nanogel-PDS-Fe_3O_4 NPs Hydrogel Nanocomposite and DOX/PDN-Nanogel-PDS-Fe_3O_4 NPs Hydrogel Nanocomposite

At first, 0.2 g of salep was dissolved in 25 mL of double distilled water with continuous mechanical stirring (200 rpm) until a homogeneous viscous mixture was obtained. Then, 4 mL of DMA solution and 5 mL of APS (0.2 g in 5 mL water) were added and the reaction mixture was stirred for 30 min. The reaction mixture was poured into 100 mL of ethanol and dried under vacuum at 40°C and then subjected to the extraction with the double distilled water as solvent to remove uncrosslinked polymer and/or residual monomer. After that, 15 mL of PDN-nanogel was added to the mixture and was stirred for 45 min. Then, the mixture was cool at room temperature and then 20 mL of $FeCl_3/FeCl_2$ (0.48/0.16 in 20 mL water) was added drop wise at room temperature. After 30 min stirring, NH_4OH (20.0 mL) was added to the mixture. Extracted sample was dried again in a vacuum and was stored in the absence of moisture, heat, and light to further characterization.

The same method was used to prepare DOX/PDN-nanogel-PDS-Fe_3O_4 NPs hydrogel nanocomposite. The only difference was related to use DOX/PDN-nanogel instead of PDN-nanogel in above method.

Swelling Study

The swelling behavior of each sample was performed by immersing a tea bag (i.e., a 100.00-mesh nylon screen) containing 0.5 g of sample into 50 mL solution. At predetermined time intervals, it was hanged until the last drop of double distilled water was fallen down and then the swelling degree was calculated from the following equation [24]:

$$\text{Swelling degree (g/g)} = (\text{Weight of swollen gel}/\text{Weight of dried gel}) - 1.$$

Absorbency Under Load (AUL)

The swelling degree of synthesized sample under load was investigated by potting a cylindrical solid weight (Teflon, $d = 60$ mm of variable height) with desired load (applied pressure 0.3 and 0.9 psi) onto 0.5 g sample. This sample was uniformly placed on the surface of a polyester gauze which was pot in a Petri dish ($d = 118$ mm and $h = 12$ mm) containing double distilled water. The swollen samples were taken out from swelling medium and were weighed at predetermined time intervals after removing the surface adhered double distilled water. Then, the swelling degree of sample was determined using above equation.

Drug Release Studies

DOX release from DOX/PDN-nanogel and DOX/PDN-nanogel-PDS-Fe_3O_4 NPs hydrogel nanocomposite under different temperatures and pH with and without magnetic field was analyzed using the following method. Generally, 1.0 mL of DOX/PDN-nanogel and DOX/PDN-nanogel-PDS-Fe_3O_4 NPs hydrogel nanocomposite was taken into a dialysis bag. Then it was carried out in 80 mL of buffer (pH = 5.3 and 7.4) with different environment temperatures (37 and 42°C). At regular time-points, 2 mL of solution was collected and was refreshed with 2 mL of fresh buffer. The amount of DOX released was measured using UV–Vis spectrometer at 480 nm and pure DOX calibration curve.

RESULTS AND DISCUSSION

Synthesis Mechanism

The synthesis strategy of the PDN-nanogel and PDN-nanogel-PDS-Fe_3O_4 NPs hydrogel nanocomposite is outlined in Scheme 1. We first prepared PDN-nanogel by copolymerization of NIPAM and DMA monomers in the presence of APS at 80°C. By adding MBA to this solution, three dimensional polymeric network structures formed and began to growing. In this time, SDS molecules act as surfactant and separated polymeric network to form nanogel. The formation of nanogel was verified by the appearing of turbidity in the solution. In another reaction container, DMA as a monomer was grafted onto salep as a backbone by graft copolymerization process. Then, PDN-nanogel was mixed with the graft copolymer. To obtain PDN-nanogel-PDS-Fe_3O_4 NPs hydrogel nanocomposite, iron sources were inserted to the reaction mixture. The Fe ions were chelated with nitrogen and oxygen atoms of graft copolymer monomer [29–31]. By adding ammonium hydroxide, Fe_3O_4 NPs were prepared in solution and act as crosslinking agents for producing three-dimensional polymeric network of PDN-nanogel-PDS-Fe_3O_4 NPs hydrogel nanocomposite [30].

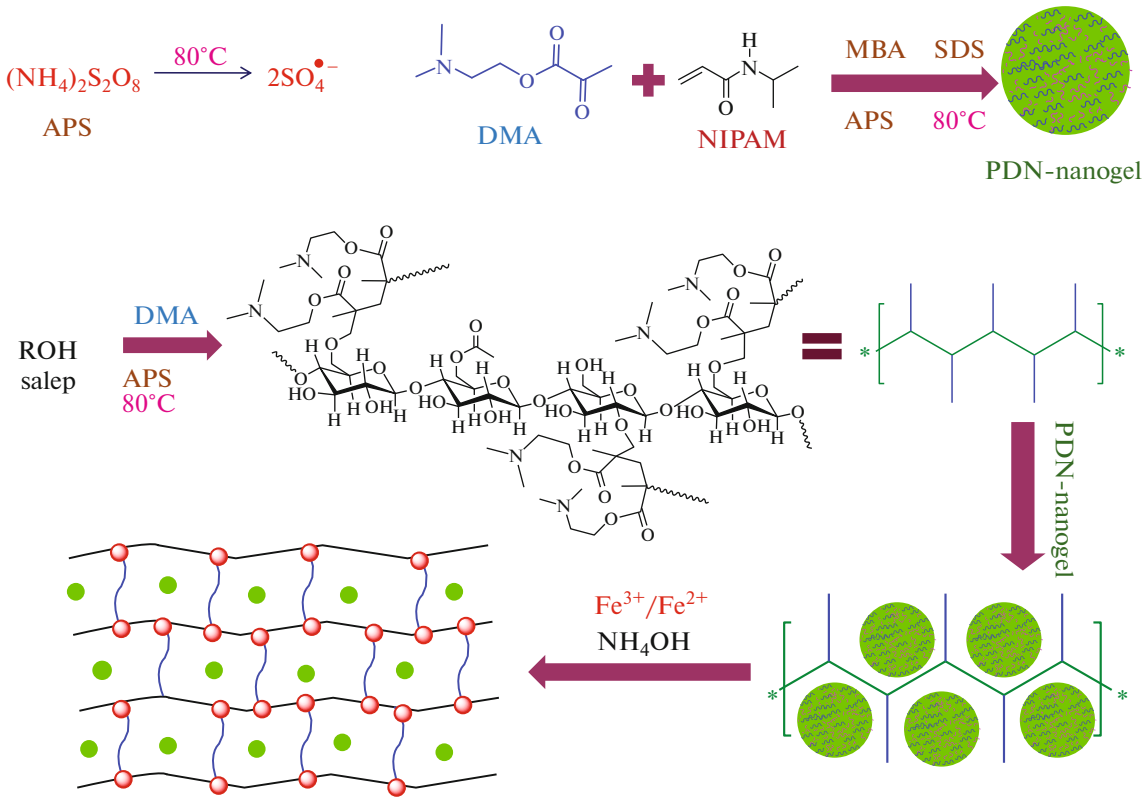

Scheme 1. (Color online).

Characterization

FTIR spectroscopy was used to characterize the molecular structure of salep, PDMA, PNIPAM, PDN-nanogel, and PDN-nanogel-PDS-Fe_3O_4 NPs hydrogel nanocomposite (Fig. 1a). The main characteristic absorption peaks in the FTIR spectrum of salep could be identified at 3265 and 1690 cm^{-1}, which were assigned to hydroxyl functional groups and stretching modes of the carboxyl groups, respectively. The FTIR spectrum of PDMA demonstrated two characteristics at 1165 and 1720 cm^{-1}, which were responsible for the stretching vibrations of dimethylamino groups and the stretching vibrations of carbonyl in the ester functional groups, respectively. The FTIR spectrum of PNIPAM showed peaks at 3500 and 1635 cm^{-1} which were assigned to N–H and carbonyl stretching of the amide groups, respectively. In the FTIR spectrum of PDN-nanogel, the peaks at 3500, 1720, 1635, and 1165 cm^{-1} were observed because of N–H stretching of the amide groups, carbonyl stretching of the amide groups, the stretching vibrations of carbonyl in the ester functional groups, and stretching vibrations of dimethylamino groups, respectively. These results implied the existence of PNIPAM and PDMA chains in the synthesized nanogel. In the FTIR spectrum of PDN-nanogel-PDS-Fe_3O_4 NPs hydrogel nanocomposite, the presence of characteristic peaks of the salep, PDMA, and PDN-nanogel confirmed the graft polymerization of PDMA chains onto salep biopolymer and successfully encapsulated of PDN-nanogel into the PDN-nanogel-PDS-Fe_3O_4 NPs hydrogel nanocomposite.

The thermal stability and thermal decomposition of salep, PDMA, PNIPAM, PDN-nanogel, and PDN-nanogel-PDS-Fe_3O_4 NPs hydrogel nanocomposite were investigated by TG analysis (Fig. 1b). The mass loss for all samples occurred in two different temperature ranges. The first decomposition step in the range of 35–100°C was attributed to water evaporation. The thermogram of salep in the second stage involved a two-step mechanism in the range of 260–650°C due to the dehydration of saccharide rings and breaking of C–O–C bonds in the polymeric chains. The main degradation stages for PDMA and PNIPAM occurred at 200–500 and 200–620°C, respectively, due to the thermal decomposition of the carboxyl and amide side groups of the polymers. These thermal decompositions cause to emission of ammonia, carbon monoxide, and carbon dioxide. The decomposition stage for PDN-nanogel started at 180°C and extended to approximately 410°C with the maximum decomposition rate at approximately 380°C. However,

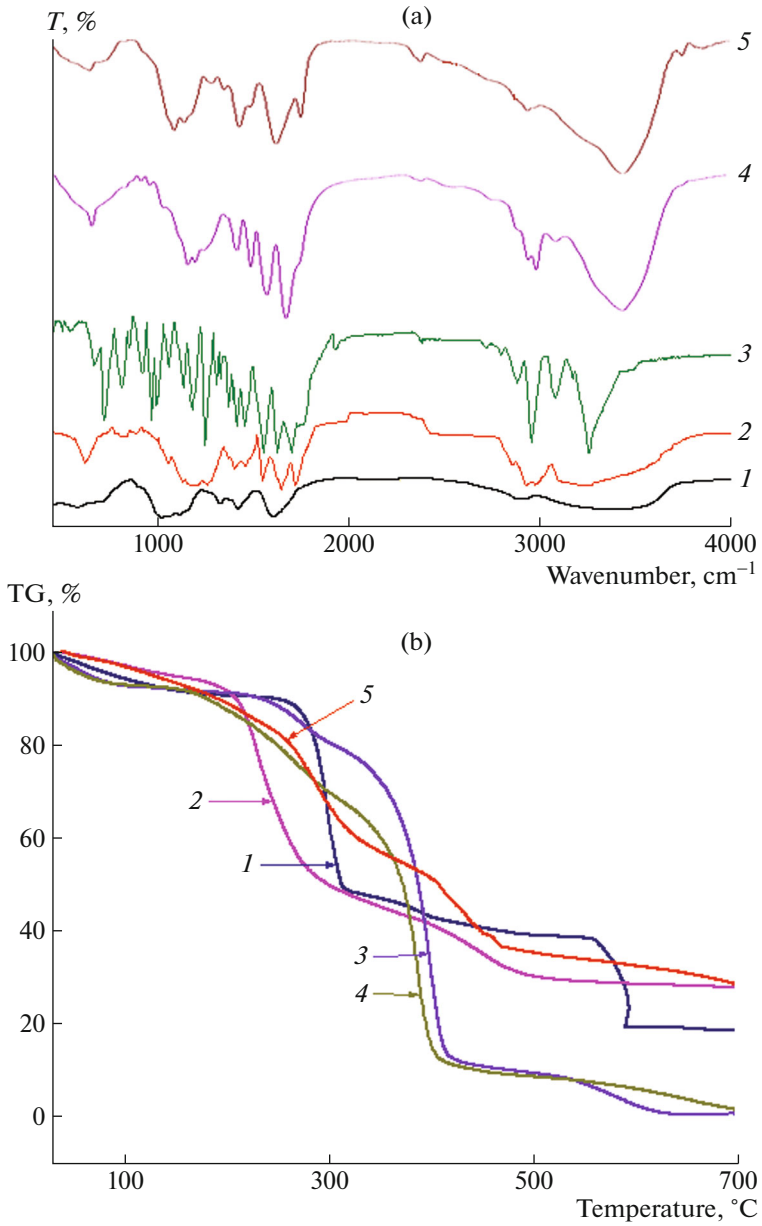

Fig. 1. (Color online) (a) FTIR spectra and (b) TG analyses of (*1*) salep, (*2*) PDMA, (*3*) PNIPAM, (*4*) PDN-nanogel, and (*5*) PDN-nanogel-PDS-Fe_3O_4 NPs hydrogel nanocomposite.

the thermal decompositions of PDN-nanogel-PDS-Fe_3O_4 NPs hydrogel nanocomposite occurred in the range of 140–480°C. The difference in decomposition between the PDN-nanogel and PDN-nanogel-PDS-Fe_3O_4 NPs hydrogel nanocomposite indicated that the incorporation of PDN-nanogel into PDN-nanogel-PDS-Fe_3O_4 NPs hydrogel nanocomposite could significantly increase thermal stability of the polymeric matrix.

The surface morphologies of PDN-nanogel and PDN-nanogel-PDS-Fe_3O_4 NPs hydrogel nanocomposite were studied by SEM images (Fig. 2). A highly porous interconnected structure could be seen in these samples. However, PDN-nanogel-PDS-Fe_3O_4 NPs hydrogel nanocomposite showed improved porosity with respect to PDN- nanogel due to the proper effecting of Fe_3O_4 NPs as a crosslinking agent and presence of salep as a polymeric backbone. These properties made PDN-nanogel-PDS-Fe_3O_4 NPs hydrogel nanocomposite as a best choose to absorb water or drug from around environment.

To more investigation about the morphology and size distribution of PDN-nanogel and Fe_3O_4 NPs, AFM of PDN-nanogel and PDN-nanogel-PDS-Fe_3O_4 NPs hydrogel nanocomposite were obtained

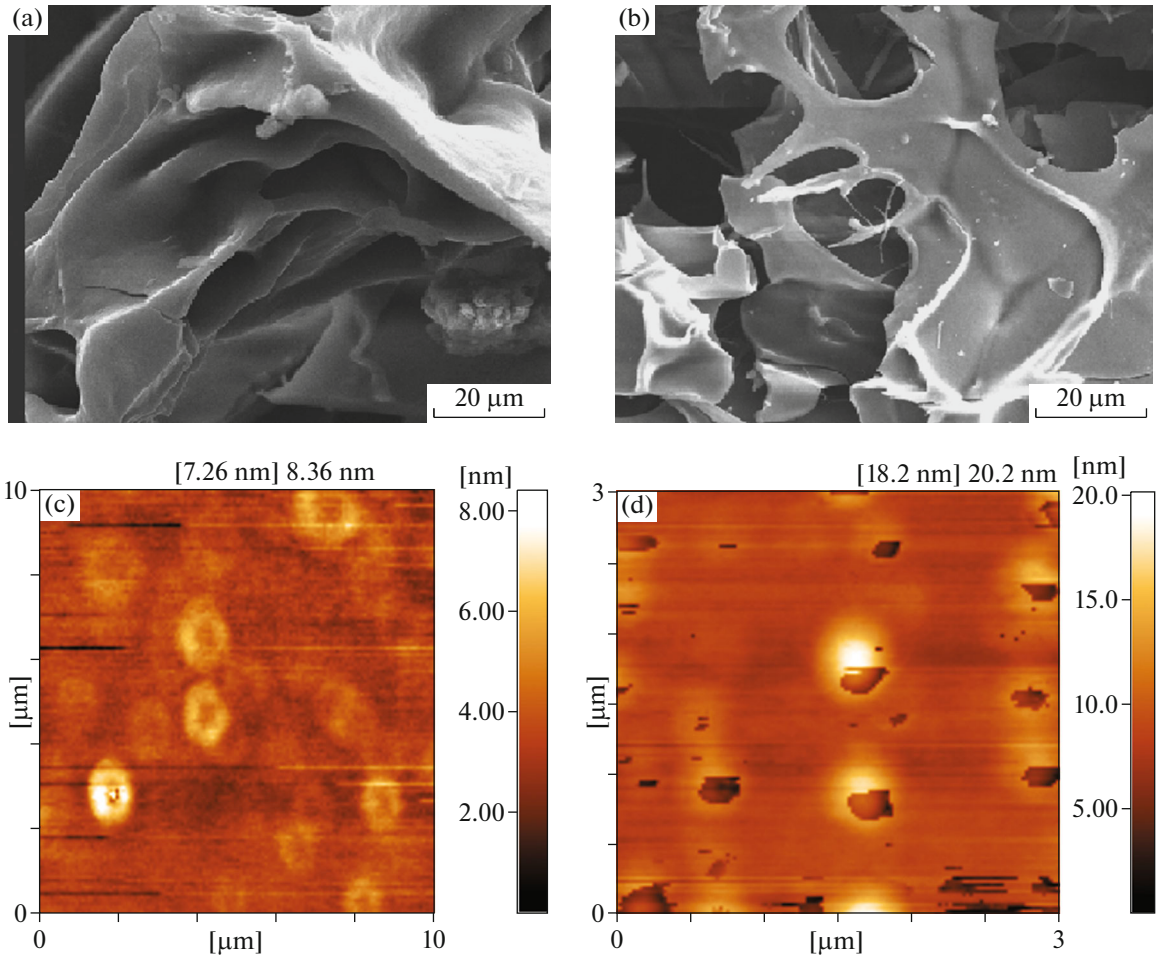

Fig. 2. (Color online) (a), (b) SEM and (c), (d) AFM of (a), (c) PDN-nanogel and (b), (d) PDN-nanogel-PDS-Fe_3O_4 NPs hydrogel nanocomposite.

(Fig. 2). Both samples showed spherical morphology with a smooth surface and diameter of about 8.36 nm for PDN-nanogel and 20.22 nm for Fe_3O_4 NPs.

To more exploration about the presence of Fe_3O_4 NPs in the PDN-nanogel-PDS-Fe_3O_4 NPs hydrogel nanocomposite sample, XRD pattern of it was survived (Fig. 3). In the XRD pattern of PDN-nanogel-PDS-Fe_3O_4 NPs hydrogel nanocomposite, some peaks at $2\theta = 30.1°$, 35.4°, 43.0°, 53.5°, 57.0° and 62.5° marked by their indices [(220), (311), (400), (422), (511), and (440)] were observed. Huang et al. reported the same results for pure Fe_3O_4 NPs [32]. Therefore, it could be confirmed that the Fe_3O_4 NPs were successfully fabricated into the hydrogel network. The size of Fe_3O_4 NPs was calculated to be ~15.51 nm by Scherrer formula.

The magnetic properties of the PDN-nanogel-PDS-Fe_3O_4 NPs hydrogel nanocomposite were studied by VSM analysis. As shown in Fig. 3, PDN-nanogel-PDS-Fe_3O_4 NPs hydrogel nanocomposite had small ferromagnetic properties due to the narrow hysteresis ring. Magnetic features such as magnetization saturation (M_s), field reversals (H_c), and residual magnetization (M_r) were calculated about 0.06 emu/g, −150–150 Oe, and −45–45 emu/g, respectively. According to the literature, these magnetization features are appropriate for biomedical applications.

Swelling Study

Swelling behavior of hydrogel has become the subject of increasing interest in many biomedical applications [23]. When a dry hydrogel material is immersed in water, water could diffuse into the pre-existing state and dynamic species between polymeric chains. Therefore, the materials get bigger and hydrogel swelled [22]. The swelling behavior of PDN-nanogel-PDS-Fe_3O_4 NPs hydrogel nanocomposite as a function of time were determined by placing 0.5 g of these samples in double distilled water at 25°C and measuring their swelling after a period. The results in Fig. 4 display that the swelling of PDN-nanogel-PDS-Fe_3O_4 NPs hydrogel nanocomposite increases with time,

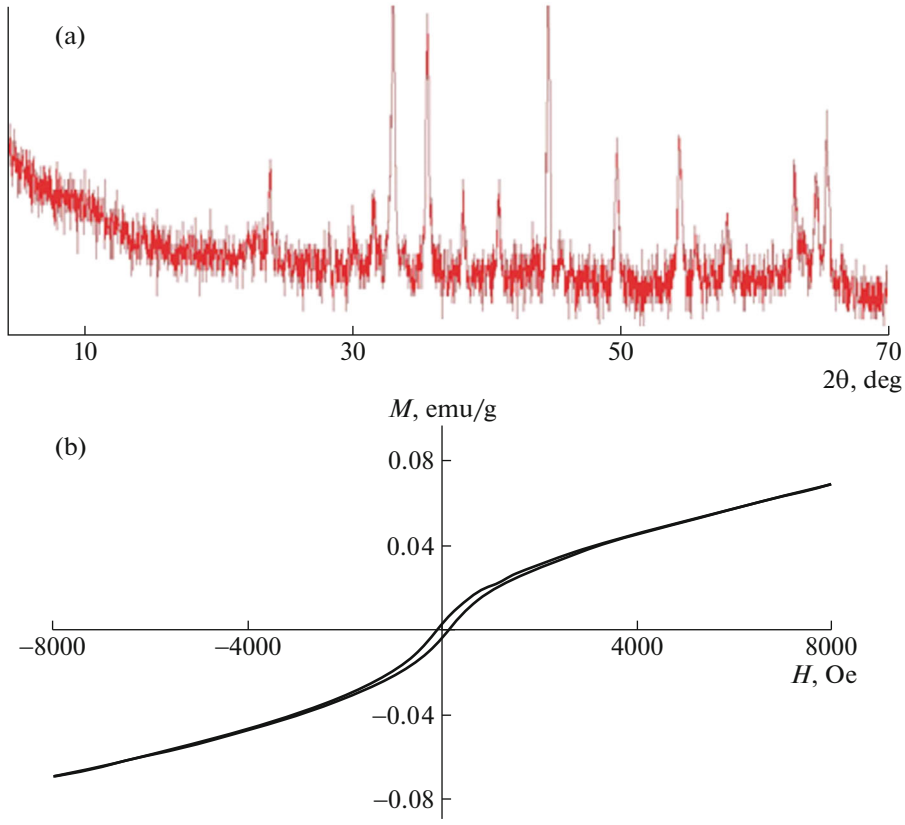

Fig. 3. (Color online) (a) XRD and (b) VSM of PDN-nanogel-PDS-Fe_3O_4 NPs hydrogel nanocomposite.

first rapidly and then slowly, reaching a maximum constant swelling after a 75 min of investigation. It is also obvious that the swelling capacity of PDN-nanogel is a very small (~57 g/g) in comparison to that of the PDN-nanogel-PDS-Fe_3O_4 NPs hydrogel nanocomposite.

The effect of AUL on swelling behavior of the PDN-nanogel-PDS-Fe_3O_4 NPs hydrogel nanocomposite in double distilled water were investigated by varying amount of pressures (0.3 and 0.9 psi) whereas the other conditions were kept constant. As shown in Fig. 4, increasing pressure decreases the swelling degree of PDN-nanogel-PDS-Fe_3O_4 NPs hydrogel nanocomposite. It was due to the decrease in the pores dimensions and simultaneously their change shape [29]. This result suggest that PDN-nanogel-PDS-Fe_3O_4 NPs hydrogel nanocomposite can swell under an applied load or controlling force and are very good in producing a variety of absorbents such as pads and diapers.

The swelling behavior of PDN-nanogel-PDS-Fe_3O_4 NPs hydrogel nanocomposite at various temperatures were observed by placing 0.5 g of this sample in double distilled water with different temperatures and examining its swelling after 75 min. As can be seen in Fig. 5a, the swelling of PDN-nanogel-PDS-Fe_3O_4 NPs hydrogel nanocomposite slightly decreased with the increasing of temperature from 20 to 45°C. It might be due to the breaking of the hydrogen-bonding interaction amongst hydrophilic groups and collapsed the polymeric network of hydrogel nanocomposite at high

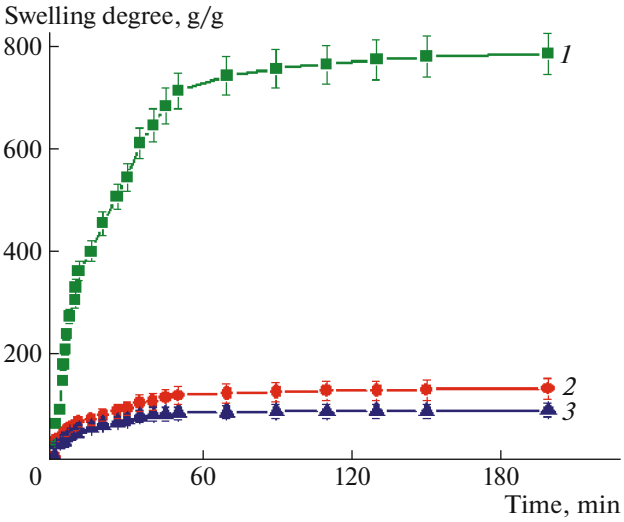

Fig. 4. (Color online) Time dependence of the swelling degree of PDN-nanogel-PDS-Fe_3O_4 NPs hydrogel nanocomposite at different pressure: (*1*) 0, (*2*) 0.3, and (*3*) 0.9 psi.

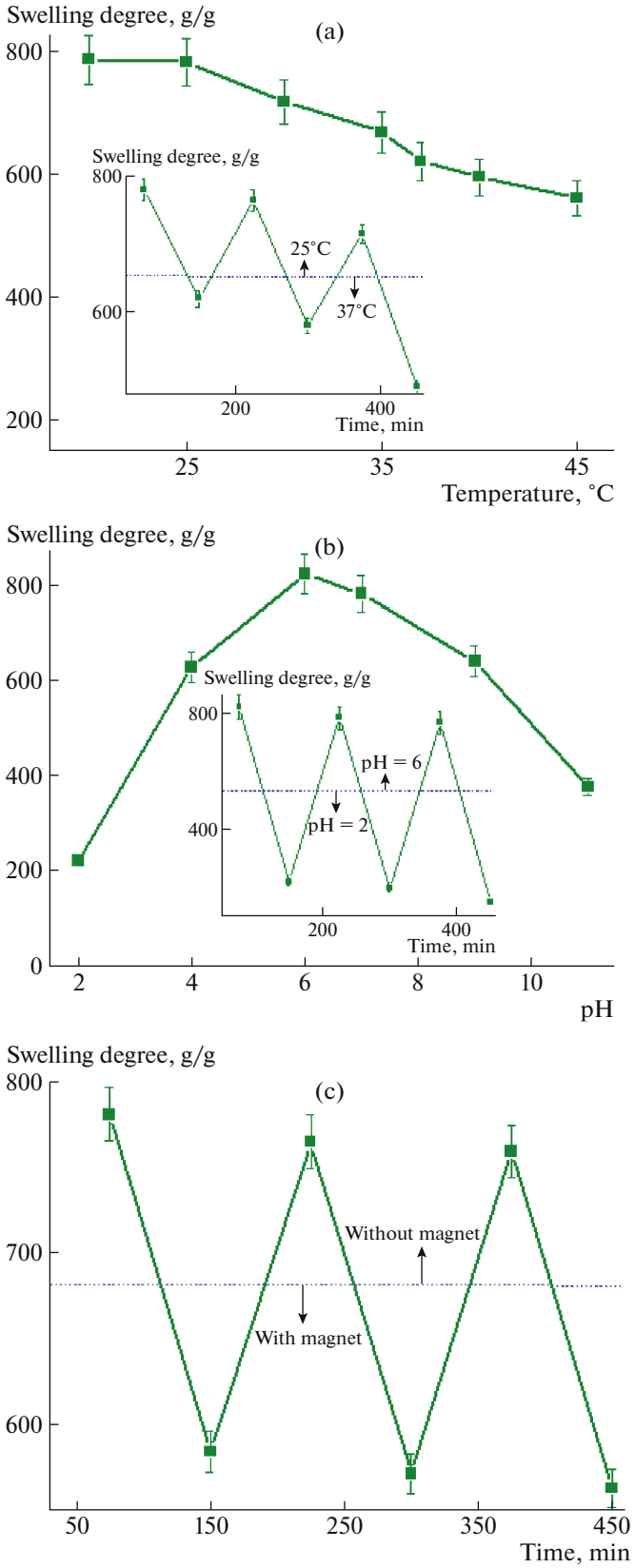

Fig. 5. (Color online) The effect of (a) temperature, (b) pH, and (c) magnetic-filed on the swelling degree of PDN-nanogel-PDS-Fe_3O_4 NPs hydrogel nanocomposite.

temperatures [30]. This data clearly indicate a temperature responsive behavior of the PDN-nanogel-PDS-Fe_3O_4 NPs hydrogel nanocomposite. In order to investigate thermo-sensitive property of PDN-nanogel-PDS-Fe_3O_4 NPs hydrogel nanocomposite, the temperature-dependent swelling reversibility was tested at 25 and 37°C and results are shown in Fig. 5a. It was observed that the PDN-nanogel-PDS-Fe_3O_4 NPs hydrogel nanocomposite had a good swelling-deswelling behavior, which repeated many times.

The pH dependent swelling behavior of PDN-nanogel-PDS-Fe_3O_4 NPs hydrogel nanocomposite at various pHs were examined by placing 0.5 g of this sample in different pH at 25°C and observing the amount of its swelling after 75 min. As shown in Fig. 5b, the swelling of sample increased with the rising of the pH from 2 to 6, however, it decreased at pH > 6. In the acid solution, the low repulsion between negatively charged carboxylate ions is responsible for the small swelling [9]. The increase of pH solution in the range 2 < pH < 6 induces high repulsion between ionic groups and consequently the swelling increased [10]. At higher pH values, the rising concentration of OH in solution dramatically decrease the osmotic pressure, restrain the extending of the tangled molecular chain of hydrogel networks and cause to decrease their swelling values [9, 10]. To examine pH-sensitive property of PDN-nanogel-PDS-Fe_3O_4 NPs hydrogel nanocomposite, the swelling-deswelling behavior was studied by alternately placing it in pH 2 and pH 6 at 25°C. As can be seen from Fig. 5b, the PDN-nanogel-PDS-Fe_3O_4 NPs hydrogel nanocomposites how reversible swelling in these pHs which is attractive for use it in the controlled delivery of drugs.

The magnetic dependent swelling behavior of PDN-nanogel-PDS-Fe_3O_4 NPs hydrogel nanocomposite in pH 6 at 25°C were examined by placing a magnet in close to the solutions containing 0.5 g of this sample and surveying the amount of its swelling after 75 min. Then, the magnet was removed and its swelling was measured after 75 min. As shown in Fig. 5c, the swelling of PDN-nanogel-PDS-Fe_3O_4 NPs hydrogel nanocomposite is decreased in the presence of magnet. This phenomenon may be attributed to the collecting of the Fe_3O_4 NPs in the neighbors of magnet [29]. It causes to reduce distance between the Fe_3O_4 NPs and produce close-packed shells of Fe_3O_4 NPs which can prevent the solution diffusion into polymeric network [31]. In addition, the excellent reversible swelling-deswelling behavior of PDN-nanogel-PDS-Fe_3O_4 NPs hydrogel nanocomposite was observed for 4 cycles, which is important advantage for their application in the field of targeted drug delivery.

Drug Release

In order to evaluate the suitability of the synthesized hydrogel nanocomposite as a stimuli-responsive

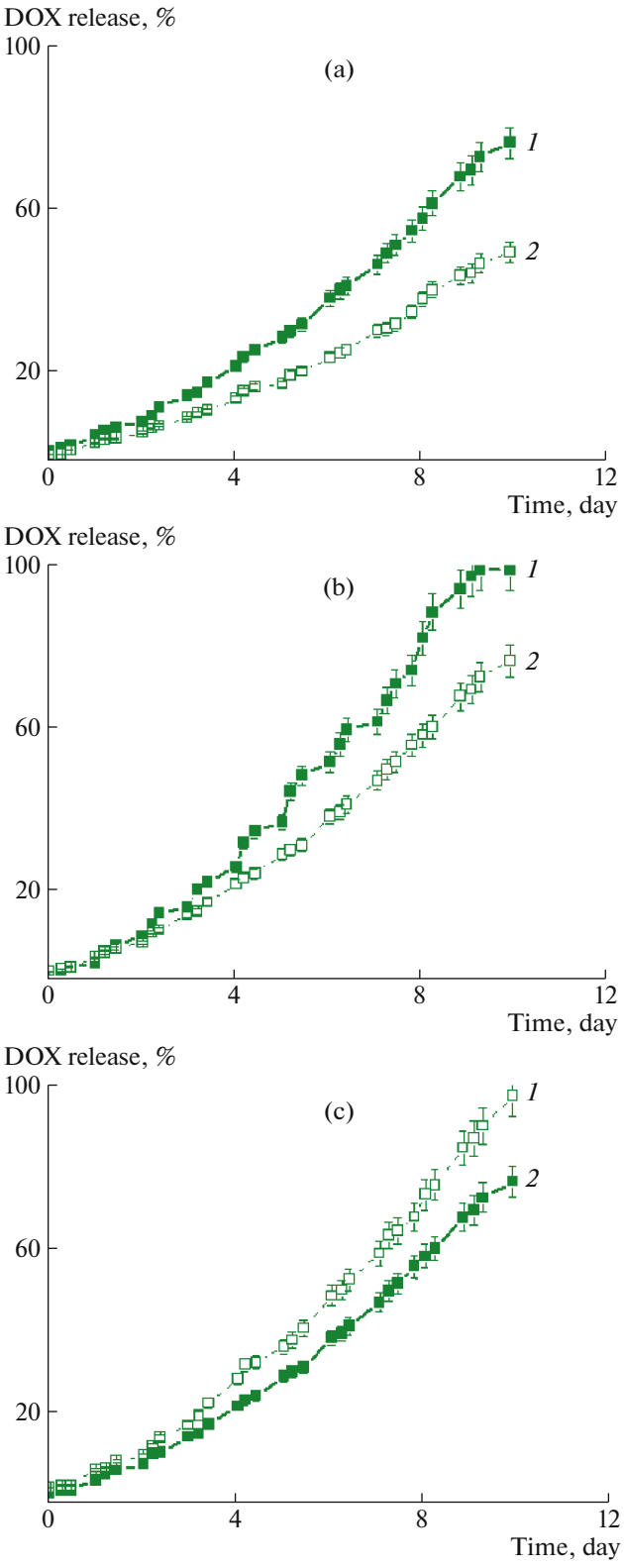

Fig. 6. (Color online) Effect of (a) pH: (*1*) 5.3 and (*2*) 7.4 (T = 37°C and without magnetic field) (b) temperature: (*1*) 42 and (*2*) 37°C (pH 5.3 and without magnetic field), and (c) magnetic field: (*1*) with and (*2*) without magnet (pH 5.3 and T = 37°C) on DOX release from PDN-nanogel-PDS-Fe_3O_4 NPs hydrogel nanocomposite.

Table 1. Regression coefficient (R^2) values of different kinetics models for DOX release from DOX/PDN-nanogel-PDS-Fe_3O_4 NPs hydrogel nanocomposite with and without magnetic field

Model	Without magnetic field	With magnetic field
Zero-order	0.89	0.87
First order	0.86	0.92
Higuchi	0.93	0.87
Hixson–Crowell	0.89	0.92
Korsemeyer–Peppas	0.98	0.98

drug delivery vehicle, the antitumor drug DOX was loaded into PDN-nanogel and then DOX/PDN-nanogel was embedded into hydrogel nanocomposite as described above. DOX loading efficiency of PDN-nanogel was approximately 81.50%, which suggesting high drug loading content.

In vitro DOX release profile from DOX/PDN-nanogel-PDS-Fe_3O_4 NPs hydrogel nanocomposite was performed under different conditions. Figure6a shows the release profiles of DOX from PDN-nanogel-PDS-Fe_3O_4 NPs hydrogel nanocomposite at 37°C in different pH values (5.3 and 7.4). According to these results, the DOX release rate dramatically accelerates when pH decrease from 7.4 to 5.3. It is probably attributed to the presence of the DMA in the polymeric structure of hydrogel nanocomposite [11]. Since cancer cells have acidic environment, these samples are good chosen for cancer treatment. Thus, they can reduce the amount of drug release in neutral environments and improve the drug target to kill the cancer cells.

To confirm the feasibility of this sample, the effect of temperature on drug release was evaluated at pH 5.3 with different temperatures and results are shown in Fig. 6b. It could be seen that the amount of drug release increased as temperature changed from 37 to 42°C. It was revealed the temperature responsive controlled release of DOX from these samples, mainly due to the shrinking of the PNIPAM shells at higher temperature [10].

Lastly, we evaluated the effect of magnetic field on drug release from this sample at pH 5.3 and $T = 37$°C (Fig. 6c). The DOX release from this sample increased in the presence of the magnetic field. This result is attributed to electrostatic repulsions between amine groups in their polymeric structure and Fe_3O_4 NPs, which destabilize polymeric structure and permit solute diffusion out-of the polymer network [31].

We also analyzed the experimental drug delivery data according to the four common models: zero order, first order, Higuchi, Hixson–Crowell, and Korsmeyer–Peppas models in order to describe how the encapsulated drugs release from the DOX/PDN-nanogel-PDS-Fe_3O_4 NPs hydrogel nanocomposite. Therefore, we used the generalized forms of these models as the following equations for fitting the drug release data [9–12].

Zero-order model: $M_0 - M_t = k_0 t$,

First order model: $\ln(M_t - M_0) = -k_1 t$,

Higuchi model: $M_t = k\sqrt{t}$

Hixson–Crowell model: $(M_0)^{1/3} - (M_t)^{1/3} = kt$,

Korsemeyer–Peppas: $M_t/M_\infty = kt^n$,

where t is the sampling time; M_t and M_∞ represent the cumulative drug mass released out at time t and infinity, respectively; k is the drug release rate constant, and n display the release mechanism. If $n \le 0.45$, drug transport is controlled by diffusion and it is called Fickian diffusion. If $0.45 < n < 0.89$, the drug transport is resulted from the collaborative effect of diffusion and macromolecular relaxation. If $n \ge 0.85$, the drug transport is resulted from case-II transport [9–12]. All release parameters of these four models with related regression coefficient (R^2) are listed in Table 1. According to the obtained R^2, it can be confirmed that the Korsmeyer–Peppas model best fits with the experimental data for DOX released from DOX/PDN-nanogel-PDS-Fe_3O_4 NPs hydrogel nanocomposite with and without magnetic field. The amount of n for DOX release from DOX/PDN-nanogel-PDS-Fe_3O_4 NPs hydrogel nanocomposite in the pH 5.3, $T =$ 37°C, and without magnetic field was about 0.84 which indicated the collaborative effect of diffusion and macromolecular relaxation for DOX release. The amount of n for DOX release from DOX/PDN-nanogel-PDS-Fe_3O_4 NPs hydrogel nanocomposite in the pH 5.3, $T = 37$°C, and with magnetic field was about 1.39 which indicated the case-II transport for DOX release. Therefore, the DOX releases in these conditions are controlled by polymer structure.

CONCLUSIONS

In summary, a novel drug delivery system was synthesized by incorporation of PDN-nanogel into pH, thermo, and magnetic responsive PDS-Fe_3O_4 NPs hydrogel nanocomposite. FTIR spectra and TG analyses studies confirmed the successfully preparation of PDN-nanogel-PDS-Fe_3O_4 NPs hydrogel nanocomposite. SEM images showed the porous structure of prepared hydrogel nanocomposite. The VSM results exhibited the magnetic properties of prepared sample. AFM results showed spherical morphology with a smooth surface for obtained samples. In addition, the synthesized PDN-nanogel-PDS-Fe_3O_4 NPs hydrogel nanocomposite showed considerable ability to DOX release at pH 5.3 and 42°C in the presence of magnetic field. Therefore, it is reasonable to say that the PDN-nanogel-PDS-Fe_3O_4 NPs hydrogel nanocomposite is promising for drug delivery systems.

ACKNOWLEDGMENTS

The authors wish to thank Payame Noor University for their financial support of this study.

REFERENCES

1. I. Prieto, S. Montemuiño, J. Luna, M. V. Torres, and E. Amaya, Clin. Nutr. **36**, 1457 (2017).
2. W. Tsai, H. Tsai, Y. Wong, J. Hong, S. Chang, and M. Lee, Mater. Sci. Eng., C **82**, 317 (2018).
3. M. J. Duffy, N. C. Synnott, and J. Crown, Eur. J. Cancer **83**, 258 (2017).
4. A. Shahrokni, A. J. Wu, J. Carter, and S. M. Lichtman, Clin. Geriatr. Med. **32**, 63 (2016).
5. J. Zugazagoitia, C. Guedes, S. Ponce, S. Molina-Pinelo, and L. Paz-Ares, Clin. Ther. **38**, 1551 (2016).
6. K. P. Medina-Alarcón, A. R. Voltan, B. Fonseca-Santos, I. Jacob Moro, and A. M. Fusco-Almeida, Mater. Sci. Eng., C **80**, 748 (2017).
7. N. Sabbagh, A. Akbari, N. Arsalani, B. Eftekhari-Sis, and H. Hamishekar, Appl. Clay Sci. **148**, 48 (2017).
8. G. Cavallaro, G. Lazzara, M. Massaro, S. Milioto, R. Noto, F. Parisi, and S. Riela, J. Phys. Chem. C **119**, 8944 (2015).
9. N. A. Peppas and D. S. V. Blarcom, J. Controlled Release **240**, 142 (2016).
10. E. Mauri, F. Rossi, and A. Sacchetti, Mater. Sci. Eng., C **61**, 851 (2016).
11. M. Saboktakin and R. M. Tabatabaei, Int. J. Biol. Macromol. **75**, 426 (2015).
12. W. Wei, J. Li, X. Qi, Y. Zhong, G. Zuo, X. Pan, T. Su, J. Zhang, and W. Dong, Carbohydr. Polym. **177**, 275 (2017).
13. G. R. Bardajee and Z. Hooshyar, J. Polym. Res. **20**, 67 (2013).
14. J. Xu, M. Tam, S. Samaei, S. Lerouge, J. Barralet, M. M. Stevenson, and M. Cerruti, Acta Biomater. **48**, 247 (2017).
15. G. R. Bardajee, Z. Hooshyar, F. Zehtabi, and A. Pourjavadi, Iran. Polym. J. **21**, 829 (2012).
16. Y. Ren, X. Zhao, X. Liang, P. X. Ma, and B. Guo, Int. J. Biol. Macromol. **105**, 1079 (2017).
17. C. Gao, J. Ren, C. Zhao, W. Kong, Q. Dai, Q. Chen, C. Liu, and R. Sun, Carbohydr. Polym. **151**, 189 (2016).
18. J. Hu, Y. Chen, Y. Li, Z. Zhou, and Y. Cheng, Biomaterials **112**, 133 (2017).
19. Z. Zhao, H. Xie, Y. Li, and Y. Jiang, J. Drug Delivery Sci. Technol. **35**, 184 (2016).
20. M. S. Gil, T. Thambi, V. H. G. Phan, S. H. Kim, and D. S. Lee, J. Mater. Chem. B **5**, 7140 (2017).
21. M. Molinos, V. Carvalho, D. M. Silva, and F. M. Gama, Biomacromolecules **13**, 517 (2012).
22. S. Lehmann, S. Seiffert, and W. Richtering, J. Am. Chem. Soc. **134**, 15963 (2012).
23. S. Sood, V. K. Gupta, S. Agarwal, K. Dev, and D. Pathania, Int. J. Biol. Macromol. **101**, 612 (2017).
24. H. S. Samanta and S. K. Ray, Carbohydr. Polym. **106**, 109 (2014).
25. R. Barbucci, G. Giani, S. Fedi, S. Bottari, and M. Casolaro, Acta Biomater. **8**, 4244 (2012).
26. M. Czaun, L. Hevesi, M. Takafujia, and H. Ihara, Chem. Commun. **2008**, 2124 (2008).
27. N. Movagharnezhad and P. N. Moghadam, Polym. Bull. **74**, 4645 (2017).
28. L. Zhou, B. He, and F. Zhang, ACS Appl. Mater. Interfaces **4**, 192 (2012).
29. G. R. Bardajee, Z. Hooshyar, and F. Rastgo, Colloid Polym. Sci. **291**, 2791 (2013).
30. G. R. Bardajee, Z. Hooshyar, M. J. Asli, F. E. Shahidi, and N. Dianatnejad, Mater. Sci. Eng., C **36**, 277(2014).
31. G. R. Bardajee and Z. Hooshyar, J. Polym. Res. **20**, 298 (2013).
32. K. Huang and S. H. Ehrman, Langmuir **23**, 1419 (2007).